RESEARCH ARTICLE

Analysing of atmospheric conditions and their effects on air quality in Istanbul using SODAR and CEILOMETER

Veli Yavuz[1] · Cem Özen[1] · Özkan Çapraz[1] · Emrah Tuncay Özdemir[2] · Ali Deniz[1,3] · İbrahim Akbayır[1] · Hande Temur[1]

Abstract

In this study, first, air pollution that is caused by the air pollutants' concentration exceeding the limit value in Istanbul between 2017 and 2020 were analysed. In addition to this analysis, the effects of meteorological parameters on pollution were also examined within the same period of time. Second, for a 14-day period during which the concentration values of the air pollutants were calculated higher than the standards, therefore, were selected as an episode. In that respect, measurements of both pollutant and meteorological parameters were obtained from air quality monitoring stations. The Weather Research and Forecasting (WRF) model was used to examine the changes of meteorological parameters in the surface and upper atmospheric levels. The cross-correlation function (CCF) was performed together with both air quality monitoring station and the WRF model output data to examine the effects of temporal changes in meteorological parameters on air pollutant concentrations on a temporal scale. In addition, some meteorological parameters were obtained from remote sensing systems (SODAR and Ceilometer). Finally, with the help of the trajectory analysis model, it was determined whether the pollutant parameters were transported or not. Consequently, within a 3-year period, the most critical parameters in terms of pollution throughout the city were assessed as NO_2 and PM_{10}. Moreover, low wind speeds and high pressure values during the episode prevented the dispersion of pollutants and caused air pollution in Istanbul.

Keywords Air pollution · Istanbul · SODAR · Ceilometer · WRF model · HYSPLIT System

Introduction

Urban air pollution is an incident that transpires as a result of industrialization in developed and developing countries. It has negative effects on the atmosphere and environment, also threatens human health (Gurjar et al. 2008; Çapraz et al. 2016, 2017; Özdemir et al. 2018; deSouza 2020; Maciejewska 2020). Migration to cities and having a higher birth rate than death rate is one of the main reasons that cause urban air pollution (Liu and Yu 2020). According to the estimates made by the United Nations (UN), the world population is expected to be 8.1 billion by 2030, and approximately 5 billion people are expected to live in

---

✉ Veli Yavuz
  yavuzv@itu.edu.tr

  Cem Özen
  ozenc@itu.edu.tr

  Özkan Çapraz
  caprazozkan@gmail.com

  Emrah Tuncay Özdemir
  etozdemir@gmail.com

  Ali Deniz
  denizali@itu.edu.tr

  İbrahim Akbayır
  akbayiri@itu.edu.tr

  Hande Temur
  temurhande@gmail.com

[1] Department of Meteorological Engineering, Istanbul Technical University, Maslak 34469 Istanbul, Turkey

[2] Turkish State Meteorological Service, Ataturk Airport Meteorology Office, 34149, Yesilkoy, Istanbul, Turkey

[3] Eurasia Institute of Earth Sciences, Istanbul Technical University, Maslak 34469 Istanbul, Turkey

cities (UNCSD 2001). Air pollutant emissions resulting from transportation, energy consumption, heating and all industrial activities pose a significant threat, especially in cities with a population density of over 10 million (Gurjar and Lelieveld 2005).

Air pollution and how they affect cities have been studied for years in the literature. These studies include Global model studies (Gurjar and Lelieveld 2005; Lawrence et al. 2007; Spiridonov et al. 2020), statistical analysis of pollutant emissions over many years (Guttikunda et al. 2003) and index studies (Stieb et al. 2005). Avdakovic et al. (2016) analysed the effects of meteorological parameters such as wind speed, humidity, temperature and pressure on the concentration of the PM_{10} in the city of Sarajevo. Li et al. (2015) analysed how the concentration values of PM_{10}, $PM_{2.5}$ and $PM_{1.0}$ change depending on meteorological factors in the Sichuan region. There are also studies examining the effects of atmospheric parameters and conditions on pollutant concentrations and distributions in Turkey and around the world. One of these parameters is an inversion, which is short for temperature inversion, occurs when the air is clear, calm and slightly windy under high pressure conditions. When these conditions emerge, since dispersion cannot transpire, the concentrations of air pollutants increase and eventually air pollution develops (Schafer et al. 2009). Generally, these conditions are observed in Istanbul during the winter and summer. Predominantly, stable atmospheric conditions were observed in the winter and in the summer. In the spring and autumn, generally unstable atmospheric conditions prevail. In the study conducted by Öztürk (2017), inversion types were analysed and their effects on air pollutants were examined. Within this framework, evaluations were presented on how the cloud structure and the changes in wind speeds/directions along the vertical atmosphere column could be effective.

Many studies have been conducted examining the effects of atmospheric boundary layer (ABL) structure on air quality. Kallistratove and Coulter (2004) used the Sonic Detection and Ranging (SODAR) to examine the variation of air pollution under stable and unstable atmospheric conditions, and analysed the medium-scale turbulence structure of vertical atmosphere. Gera et al. (2000) analysed the mixing layer height (MLH), average horizontal wind speed and vertical wind speed using the SODAR. He ascertained the effects of the changes in the mentioned parameters on O_3, CO and SO_2 concentrations. In many other similar studies, SODAR and the Light Detection and Ranging (LIDAR) have been used to examine the structure of the atmosphere and to determine the effect of changes in the pollutant concentrations (Coulter 1979; Devera et al. 1995; Beyrich and Görsdorf 1995; Marsik et al. 1995; Keder et al. 2002; Emeis et al. 2004; Angevine and Senff 2015).

Freedman et al. (2001) studied the ABL and the clouds over Orange, Massachusetts and Harvard by using the Ceilometer. As a result of their observations, they decided that there was a positive relationship between cumulus clouds observed in the boundary layer and the amount of CO_2 concentration. Teixeira and Hogan (2002) investigated cloud types in the sub-tropical ABL in order to make climate evaluations with Ceilometer. Schafer et al. (2009) calculated the height of mixing at an airport in Mexico City using the Vaisala LD40 Ceilometer. They investigated the relationship between pollutants such as NO, NO_x, CO, O_3 and meteorological parameters like wind speed-direction, temperature and radiation. As a result of their examinations, they found out that there was a relationship between the MLH and the changes in meteorological parameter values. Peng et al. (2017) analysed the ABL with the Vaisala CL51 Ceilometer for Shanghai, China. Boundary layer height was investigated by comparing the data obtained from the Ceilometer with the data from the radiosonde.

In this study, in addition to the numerical weather forecast models, air quality station data, HYSPLIT system, sounding and vertical atmospheric data methods which are used in studies on air pollution and atmosphere interaction both for the specified region and for everywhere on the world, two different remote sensing systems (SODAR and Ceilometer) were used and the functionality of these systems was analysed. The original part of the study is on analyses of multivariate. The concentration data of PM_{10}, $PM_{2.5}$, SO_2, NO_2 and O_3 pollutants were obtained from two different air quality stations in Istanbul between June 1, 2017 and June 30, 2020. Moreover, some of the meteorological parameters (actual temperature, air pressure, relative humidity, wind speed and direction) measured at surface level were also obtained from these stations. During the selected episode (a period of several days to several weeks in which high pollutant concentrations were observed), the Ceilometer was used to determine cloud coverage and cloud base heights, and the SODAR was used for collecting wind speed and direction data. Weather Research and Forecasting (WRF) model was used to provide all surface and upper level meteorological parameters on the designated episodic days. Also, The Hybrid Single-Particle Lagrangian Integrated Trajectory (HYSPLIT) model system was used to obtain more detailed information about transportation of pollutants during the episode. The first results obtained from the examinations in the study were as follows; during the episode, dust transported from the Sahara Desert caused a rise in PM concentrations. This variation in concentration was revealed in the trajectory analysis. WRF model outputs and wind speed/direction information obtained from the SODAR showed high consistency with the sounding data, indicating that it would be appropriate to use the portable SODAR system and WRF model for determining wind conditions in locations

where sounding measurements are not used. With the help of the information about the increases and decreases in the concentration levels of the pollutants in that region provided by the Ceilometer, the height of the mixing layer and especially the inversion layer, if any, was assessed.

Data and methodology

Study area

Istanbul is the most developed city in Turkey in terms of population density and urbanization, and is located between the Marmara Sea and the Black Sea. The city is located on an area of 5400 km^2, and the Bosphorus (about 30 km) which connects the Asian and European Continents is also here. A large enclosed sea to the north of the city and a smaller enclosed sea to the south also play a prominent role in weather and climate conditions. The prevailing wind direction in the city is north east and south west. Local land-sea breezes that stem from air-sea interaction can also be observed in the city. Summers are warm-hot and dry, and it rains a lot in winter months. That is to say common Mediterranean climate features are seen in the city (Unal et al. 2011). Air pollution is one of Istanbul's major problems conduced by the negative effects of

industrialization and non-stop construction around the city in which approximately 16 million people live, and industrialization has been a threat to human health since the beginning of the twentieth century. Industry, domestic heating and traffic-induced emissions are the main reasons why Istanbul's air quality is deteriorating as time progresses. Also, due to the development of industrialization in neighboring provinces, the air pollutants coming from these regions by short or long distance transport occasionally cause serious decreases in air quality (Çapraz and Deniz 2020). There are 3 airports in the city, and considering the Bosphorus, emission concentrations increase as a result of combustion activities related to both air and sea transportation. The most important emission sources seen in the city were identified as particulate matters (especially PM_{10} and $PM_{2.5}$) and NO_x (Çapraz and Deniz 2020; İncecik and İm 2012).

Within the scope of this study, measured concentration values of air pollutants and measured meteorological parameters were obtained from the stations in Sirinevler and Kagithane districts. Sirinevler district is located on the European side and north of the Marmara Sea and Kagithane district is located on a part of the European side close to the Bosphorus. Similarly, SODAR, one of the local remote sensing systems used in the study, has been located in the west of Istanbul Airport, in the south of
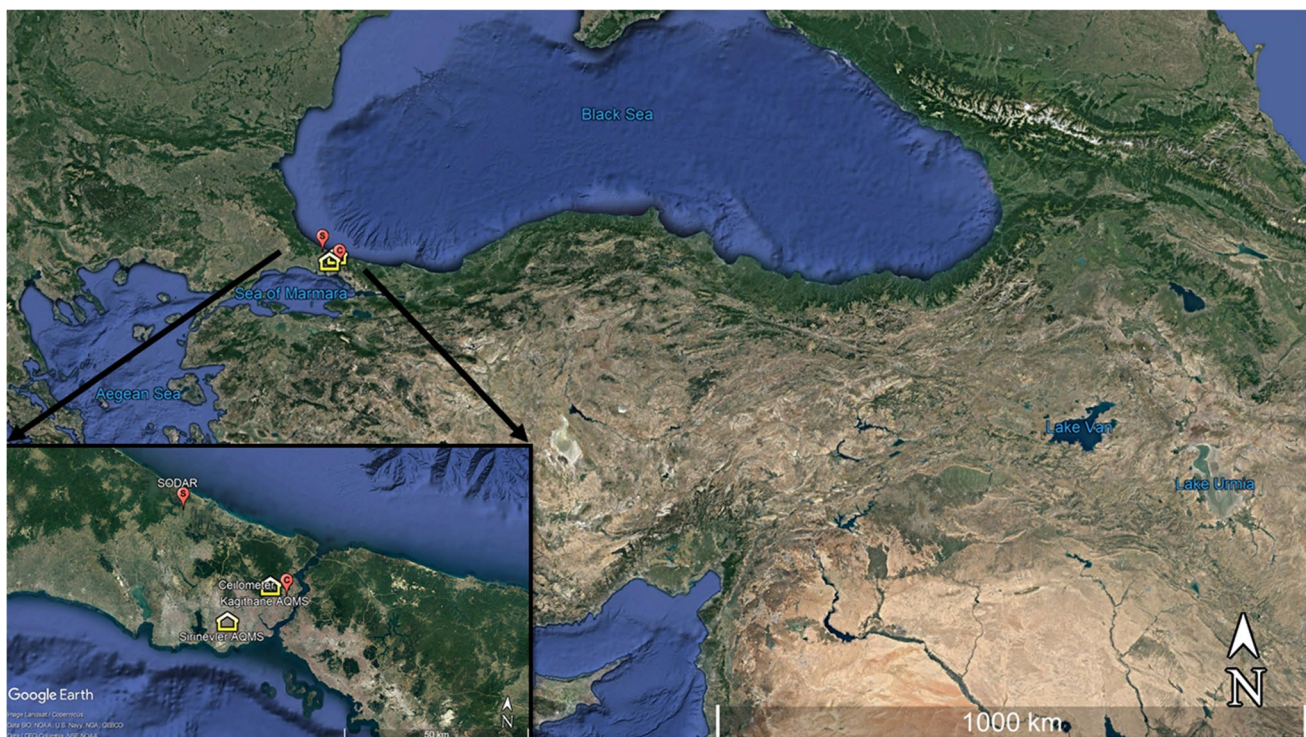

Fig. 1 The locations of the air quality measurement stations and remote sensing devices (SODAR and Ceilometer)

the Black Sea and the Ceilometer, second remote sensing system, has been located close to the Bosphorus (Fig. 1).

Data

Air pollutants

The first dataset used in the study were the concentration values of air pollutants. These data were obtained from Kagithane and Sirinevler Air Quality Measurement Stations and these stations are affiliated to the Republic of Turkey Ministry of Environment and Urbanization. Likewise, measurement data of meteorological parameters at surface level were obtained from these stations. Data of $PM_{2.5}$, SO_2, NO_2 and O_3 pollutant parameters were obtained from Kagithane Air Quality Measurement Station (AQMS) (41°05′43″N, 28°58′17″E; Altitude: 96 m). PM_{10} pollutant parameter data was obtained from Sirinevler AQMS (41°00′09″N, 28°50′19″E, Altitude: 34 m) (Fig. 1).

The measurement values of air pollutants and meteorological parameters from Kagithane and Sirinevler AQMSs were provided between June 1, 2017 and June 30, 2017. Features of the devices that measure the concentrations of pollutants at the forementioned stations are as follows:

- NO-NO_2-NO_x (Nitrous oxide) Analyser, measurement range: (between 0–50 parts per billion-ppb and 0–100 parts per million-ppm)
- SO_2 Analyser, measurement range: (0, 0.05, 0.1, 0.2, 0.5, 1, 2 and 10 ppm)
- Dust measuring device (PM_{10}, $PM_{2.5}$), measurement range: (0 to 2500 µg/m³)
- O_3 measuring device, measurement range: (between 0–50 ppb and 0–200 ppm) (IMM (İstanbul Metropolitan Municipality) Environmental Protection and Control Department, 2020)

SODAR data

The PA-0 SODAR that was manufactured by the Remtech company was the first remote sensing system used in this study. SODAR device multi-directionally emits short sound waves at sound frequencies between 1500 and 10,000 Hz into the atmosphere. These transmitted sound waves are scattered and reflected depending on the temperature of the atmosphere, wind speed and humidity. These reflected waves of different velocity and amplitude are collected by the SODAR and accumulated for analysis. The sound waves sent to the atmosphere spreads freely in the air until it coincides with a different layer (Signal 1993). The device has the capacity to measure from 15 to 700 m; required atmospheric conditions for device to reach maximum altitude (700 m) are

15 °C air temperature and 70% relative humidity. The device has wireless fidelity (WIFI), global positioning system (GPS), two-dimensional inclinometer, pressure, humidity and temperature sensors. Also, the device can be controlled remotely via WIFI (Remtech 2020).

Within the scope of the study, first, a suitable location for the SODAR was selected then the device was placed next to the transformer centre in the Terkos Dam (41°18′19″N, 28°39′38″E; Altitude: 37 m) affiliated to the Istanbul Water and Sewerage Administration (IWSA) (Fig. 1). The data were obtained from the SODAR at 30 m, 60 m, 90 m, 120 m and 240 m. Because of the distortions in the data received at the 480 m, the data of this level were not evaluated. Wind speed has been obtained at five vertical levels and in m/s unit with a 10-min time–frequency. Then the analyses were made by taking hourly averages of wind speed in the study. Wind direction values were provided in degrees for the same vertical levels.

Ceilometer data

The CBME80B Cloud Ceilometer manufactured by BIRAL company was the second remote sensing system used in this study. The Ceilometer was designed based on pulsed low power diode laser technology and LIDAR technology. The device basically sends short, powerful laser pulses in vertical direction. The emitted pulses are then reflected back by clouds, precipitation or other obstacles. The pulses coming back to the device after reflected back are analysed and the cloud base height is assessed. The device can detect three cloud levels simultaneously and can measure from 0 m up to 7500 m. The measurement resolution is 10 m. and the report interval can be adjusted between 15 and 120 s. Even though the measurement accuracy of the device is about ± %1, it may extend up to ± %10 under difficult conditions. The ambient temperature ranges in which the device can operate is between – 40 °C and 55 °C. It has a protective system against sun rays. The size of the device is 408 mm (height) × 468 mm (width) × 234 mm (length) (Biral 2020).

The Ceilometer was placed on the roof of Faculty of Aeronautics and Astronautics at Istanbul Technical University (ITU) on account of the uninterrupted energy requirement, storage unit and cleaning of the glass plate on it (41°6′5″N, 29°1′19″E; 83 m agl.) (Fig. 1). Both cloud base height data and cloud coverage data were obtained from the Ceilometer and these data were obtained at four different vertical levels. In the cloud base height data, the first level shows the base heights of the lowest level clouds detected by the device. The data for this level was generally at 1524 m and below. At the second level, the base heights of the observed clouds were generally located at and below 305 m, since the amount of coverage at the first level was not much (when 8/8—overcast coverage is seen, thus, this level and other

levels above cannot be observed). At the third and fourth levels, the cloud base height values were obtained when there was low amount of cloud coverage at first and second levels.

In the placement of both SODAR and Ceilometer, primarily, access, energy availability, security and permission conditions were taken into consideration. The distance between the two devices is around 37 km.

Methodology

WRF-setup.

Numerical weather forecast models have a crucial role in determining the characteristics of the atmosphere, topography and earth. Using the WRF model, similar data obtained at higher resolutions from both remote sensing devices and other parameters attained from terrestrial systems were also collected in this manner for the period of time between November 7, 2019 and November 20, 2019. Many studies have revealed that high-resolution atmospheric models provide much more accurate results when representing the wind structures over complex topography (Rife and Davis 2005). In this study, high-resolution data were obtained by using WRF model in three different spatial resolutions.

The 4.1.2 version of the WRF model was used with the aim of making analysis and Kagithane AQMS was chosen as the centre point of the model. Three nested domains have been created and their spatial resolutions are 9, 3 and 1 km from coarser to the inner domains respectively (Fig. 2). ERA5 reanalysis data contain 38 vertical pressure levels, and these data were used as the initial and boundary condition that are required for the model to run (Table 1).

The WRF model was run for 14 days in total for the episode. Wind speed and direction values were obtained at 30 m, 60 m, 90 m, 120 m and 240 m levels; meanwhile, actual temperature, relative humidity, wind speed, wind direction and precipitation data were obtained at 2 m from the model.

Backtrajectory analysis

The HYSPLIT System is commonly used as an atmospheric dispersion model to determine the source points of air pollutants, and to reveal the trajectory it follows (NOAA 2020). In this study, this model was used to determine hourly concentration distributions and to create trajectory estimates. HYSPLIT System was developed by the Air Resources Laboratory of the US National Oceanic and Atmospheric Administration (NOAA), and this system was used for the period of time between November 7, 2019 and November 20, 2019. The region coordinates were marked on the map
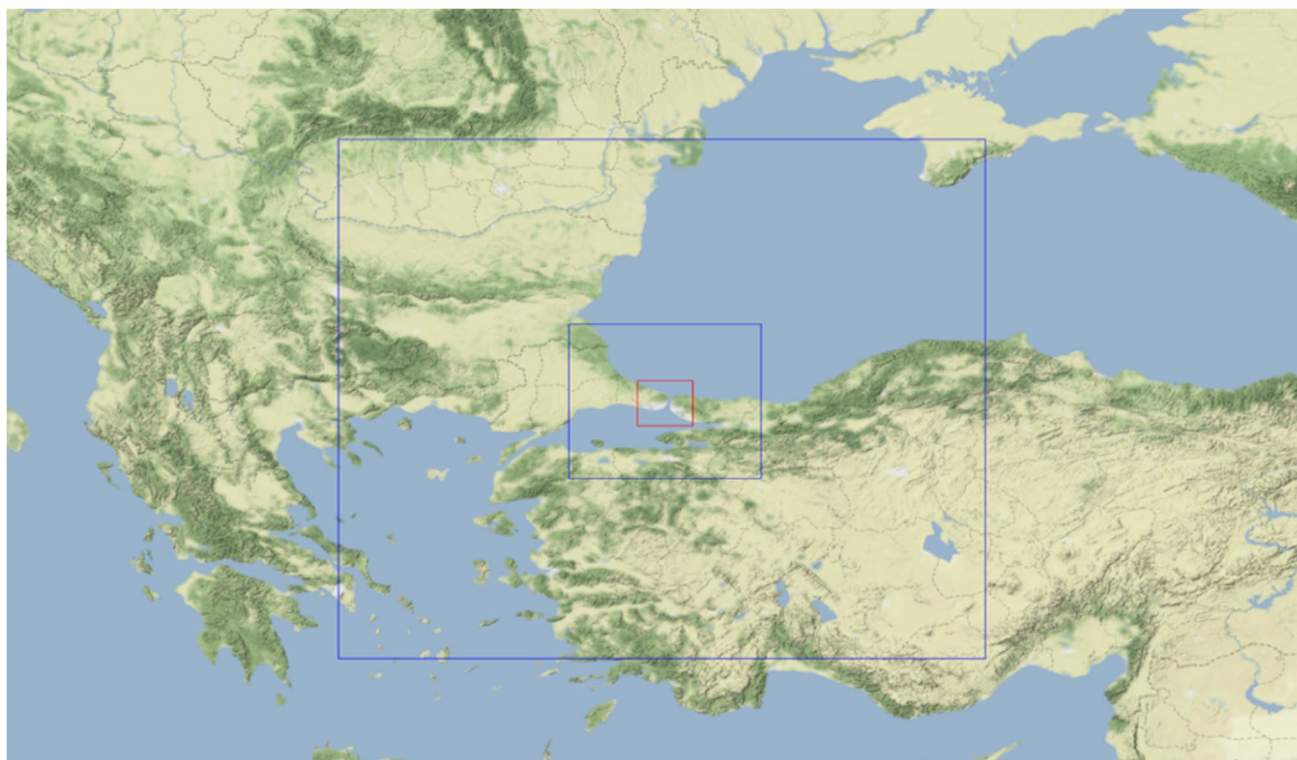

Fig. 2 WRF model study area

Table 1 WRF model configuration features

Features	Descriptions
Center point latitude, longitude (°)	41.092356, 28.974797
Domain resolutions (km)	9, 3, 1
North–East grid number	100, 88, 76
West–East grid number	100, 88, 76
Vertical number of levels	38
Microphysics	Thompson Scheme (Thompson et al. 2008)
Cumulus	Modified Tiedtke scheme (Zhang et al. 2011) (only for 9 km domain)
Longwave radiation	RRTMG (Iacono et al. 2008)
Shortwave radiation	RRTMG (Iacono et al. 2008)
Planetary boundary layer	Mellor-Yamada-Janjic TKE (Janjic 1994)
Surface-layer option	Monin–Obukhov (Janjic) (Monin and Obukhov 1954)
Land-surface option	Unified Noah land-surface model (Tewari et al. 2004)

and the historical trajectory (backtrajectory) was created and consequently maps showing dust transport were obtained.

Results

Long-term analysis results of air pollutants and meteorological parameters. Within the scope of this study, analysis of the air pollutant data was performed for approximately 37 months, within the period of time between June 1, 2017 and June 30, 2020. Statistical analyses were conducted on an hourly and daily basis (Table 2). The average PM_{10} concentration during the aforementioned period was calculated as 47.8 μg/m³ (Table 2). According to Turkey Air Quality Standards, the average daily PM_{10} limit value is 50 μg/m³, and the average annual PM_{10} limit value is 40 μg/m³. Turkish Air Quality Standard information regarding air pollutants is given in Table 3. By taking into consideration the information in Table 4 about how the limit value is exceeded, it can be concluded that PM_{10} concentrations frequently exceeds the limit value during this period. In Kagithane AQMS, the average $PM_{2.5}$ value was calculated as 25.1 μg/m³. There is no daily average $PM_{2.5}$ limit value in Turkey according to the air quality standards (MEU (Ministry of Environment and Urbanization), 2008). The average SO_2 value in Kagithane AQMS was 5.5 μg/m³, whereas according to Turkish Air Quality Standards, a daily average of SO_2 limit value is

125 μg/m³ and the average annual SO_2 limit value is 20 μg/m³ (MEU (Ministry of Environment and Urbanization), 2008). Hence, it is evident that the SO_2 values remained at very low levels during this period and remained below the limit values. The average NO_2 value in Kagithane AQMS was 65.4 μg/m³. According to Turkey Air Quality Standards, hourly average of NO_2 limit value is 250 μg/m³, and the average annual NO_2 limit value is 40 μg/m³ (MEU (Ministry of Environment and Urbanization), 2008). The measured NO_2 concentrations remained above the annual average limit value. The average O_3 value in Kagithane AQMS was 54.4 μg/m³. According to the Turkey Air Quality Standards,

Table 3 Turkish Air Quality Standards

Air pollutants	Averaging period	Turkish air quality standards
PM10	24 h	50 μg m⁻³
	1 year	40 μg m⁻³
NO2	1 h	250 μg m⁻³
	1 year	40 μg m⁻³
SO2	1 h	350 μg m⁻³
	24 h	125 μg m⁻³
O3	1 year	20 μg m⁻³
	8 h	120 μg m⁻³

Table 2 Hourly concentration values of air pollutants

	PM10 (μg/m³)	PM2.5 (μg/m³)	SO2 (μg/m³)	NO2 (μg/m³)	O3 (μg/m³)
Minimum	14.8	5.9	0.7	12.3	5.7
First quarter	33.6	15.2	2.5	46.3	37.9
Median	42.6	20.9	4.1	61.0	54.2
Average	47.8	25.1	5.5	65.4	54.4
Third quarter	55.7	30.7	7.3	80.3	70.1
Maximum	171.8	95.6	31.4	184.8	119.2

Table 4 PM$_{10}$ concentrations exceeding the limit value (Şirinevler AQMS)

Months	The number over the limit in 2017 (day)	The number over the limit in 2018 (day)	The number over the limit in 2019 (day)	The number over the limit in 2020 (day)
January	–	16	8	12
February	–	8	7	4
March	–	21	12	14
April	–	24	14	5
May	–	12	8	4
June	15	4	5	3
July	11	2	0	–
August	13	1	0	–
September	13	8	3	–
October	22	14	6	–
November	22	3	19	–
December	8	13	14	–
Total	104	126	96	42

there are no limit values for O$_3$ (MEU (Ministry of Environment and Urbanization), 2008).

Monthly analysis shows that there was a consecutive fall in PM$_{10}$ concentrations from 2017 to 2020 (Fig. 3). This decrease is thought to be the result of decline in the number of urbanization (construction) in the city, which is one of the main dust sources. No significant change was observed in PM$_{2.5}$ (Fig. 3) and NO$_2$ (Fig. 4) concentrations, and a pattern of increase in O$_3$ concentrations was observed (Fig. 4). SO$_2$ values remained at low values (Fig. 3).

The daily changes of meteorological variables such as temperature, pressure, relative humidity, wind speed and direction measured by Kagithane AQMS were examined. In the evaluations made within the designated period of time, extreme value was not observed in the daily average temperature values (not shown). Similarly, contradictions were not found in pressure and relative humidity values (not shown). Wind speed values were above average especially in winter months, and in summer months there were insignificant fluctuations in wind speed values (not shown).

Statistical analysis results

In the analysis made to examine the relationship between temperature and PM$_{10}$ values, the cross-correlation function (CCF) was used. It is the observation of correlation between two different time series x_t and y_t separated by time units. This method enables us to quantify the degree of similarity between two variables. In this study, a negative correlation was found and it was seen that while an increase in one variable was detected a decrease in the

Fig. 3 Monthly average concentration values of PM$_{10}$, PM$_{2.5}$ and SO$_2$ pollutants between June 1, 2017 and June 30, 2020. The data of PM$_{10}$ value were obtained from Kagithane AQMS, the other pollutant data were obtained from Sirinevler AQMS
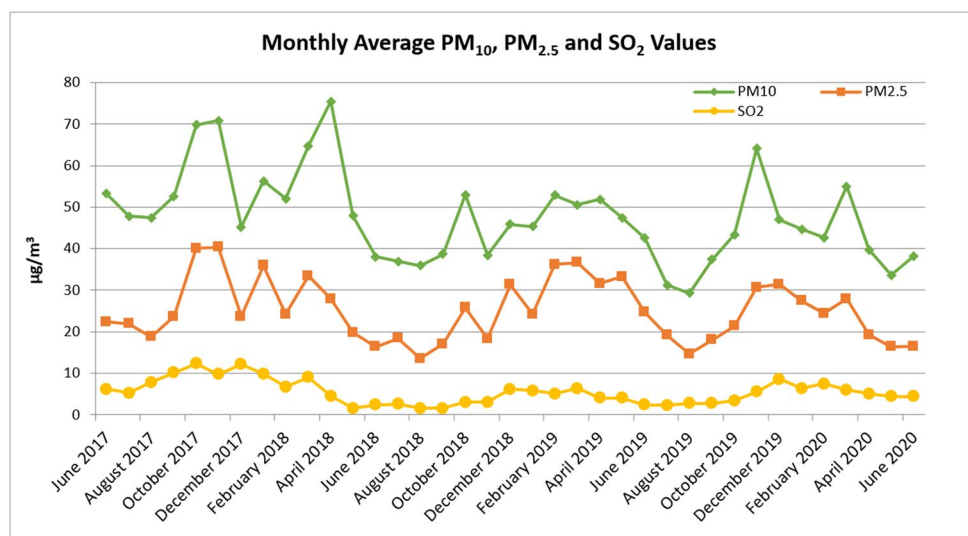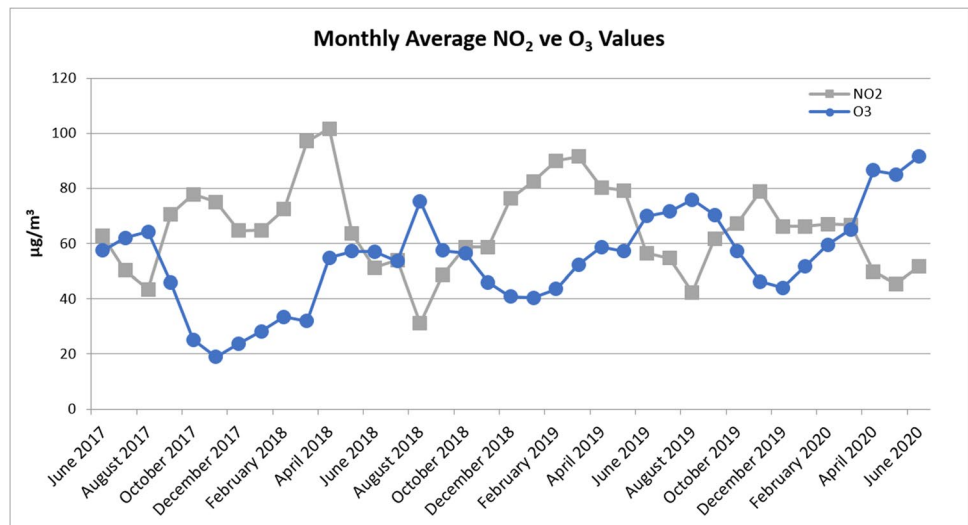
Fig. 4 Monthly average concentration values of NO$_2$ and O$_3$ pollutants, 01/06/2017–30/06/2020. Both data obtained from Kagithane AQMS

other variable was observed. In addition to this, temperatures below average were also in accordance with higher than average PM$_{10}$ values (Fig. 5).

In the analysis of the relationship between pressure values and PM$_{10}$, positive correlations were found and it was observed that high pressure values caused PM$_{10}$ values to go above average. Additionally, low pressure values were in accordance with PM$_{10}$ values below average. According to Fig. 6, the highest cross-correlation values occurred in Lag-3, Lag-2 and Lag-1. Correspondingly, high PM$_{10}$ values were measured 3, 2 or 1 day after the high pressure occurred (Fig. 6).

Analysis of the relationship between relative humidity values and PM$_{10}$ shows that humidity values above average were in accordance with PM$_{10}$ values above average. Besides, relative humidity values below average were also in accordance with PM10 values below average (Fig. 7).

In the analysis of the relationship between wind speed values and PM$_{10}$, negative correlations were found and it was seen that high wind speed values measured at surface level were in accordance with PM$_{10}$ values below the average. In addition, low wind speed values were in accordance with higher than average PM$_{10}$ values. As mentioned in the Fig. 8, the highest cross correlation values occurred in Lag-0 and Lag-1. This outcome showed that high wind speed values resulted in low PM$_{10}$ values on the day of measurement or the day after.

The episode

During the measurement period, very comprehensive analyses were made for an episode during which the pollution values reached high concentration levels. Therefore, the 14-day

Fig. 5 The CCF chart of PM$_{10}$ and actual temperature for between June 1, 2017 and June 30, 2017
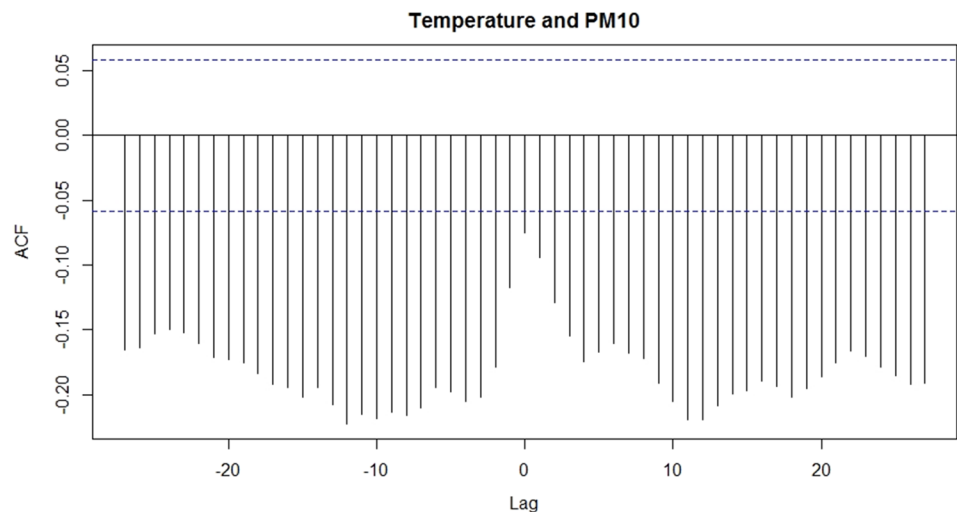
Fig. 6 The CCF chart of PM_{10} and air pressure for the period of time between June 1, 2017 and June 30, 2017
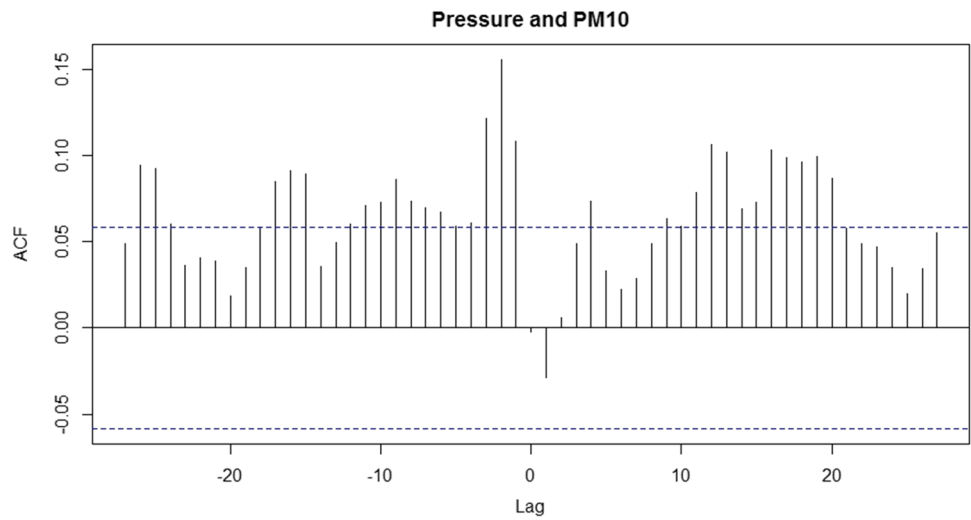

Fig. 7 The CCF chart of PM_{10} and relative humidity for the period of time between June 1, 2017 and June 30, 2017
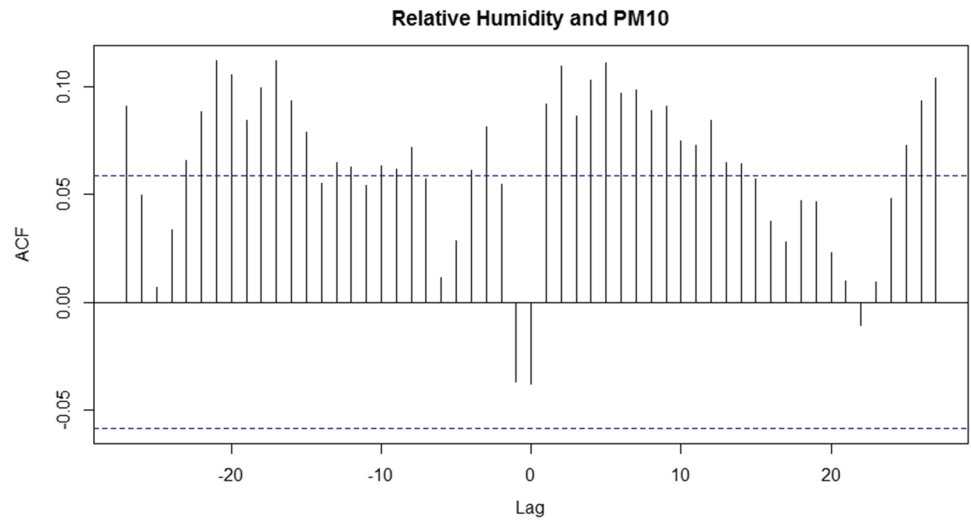

Fig. 8 The CCF chart of PM_{10} and wind speed for the period of time between June 1, 2017 and June 30, 2020
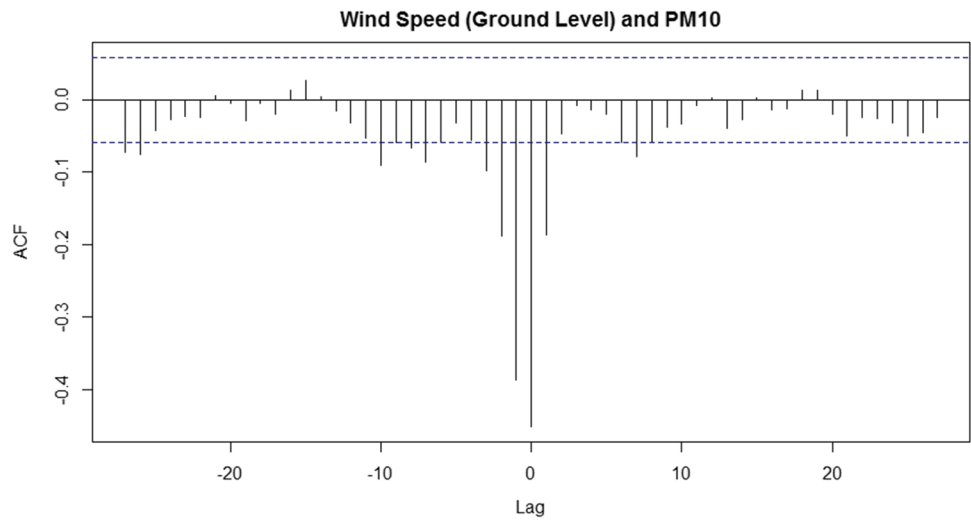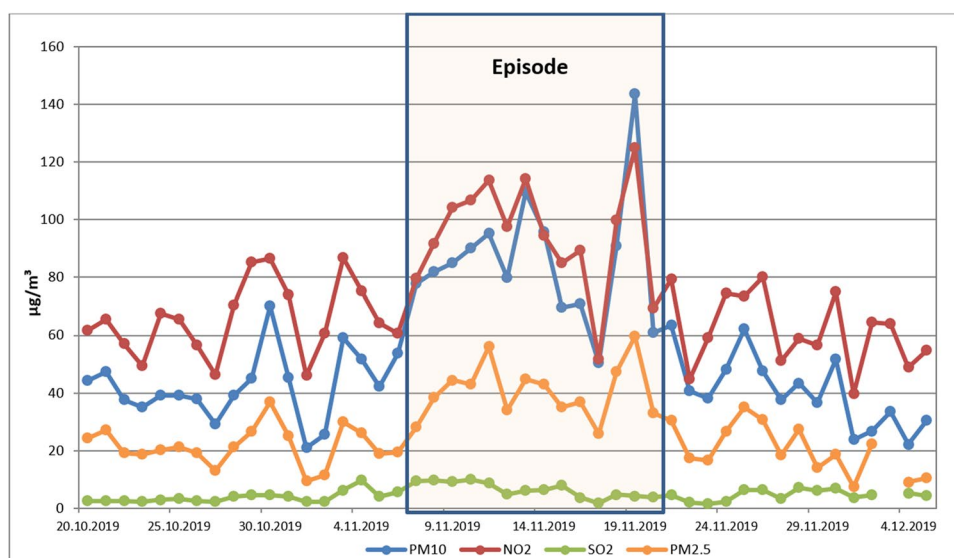
Fig. 9 Daily average values of air pollutant concentrations on the episodic days

period between November 7, 2019 and November 20, 2019 was selected as the episode (Fig. 9).

Evaluation of air pollutant concentrations

The maximum and daily average pollutant concentration were measured on a daily basis between November 7, 2019 and November 20, 2019 and they were calculated as 143.6 $\mu g/m^3$ for PM_{10} (daily average was 47.8 $\mu g/m^3$), 59.7 $\mu g/m^3$ for $PM_{2.5}$ (daily average was 25.1 $\mu g/m^3$), 10.0 $\mu g/m^3$ for SO_2 (daily average was 5.5 $\mu g/m^3$), 124.9 $\mu g/m^3$ for NO_2 (daily average was 65.4 $\mu g/m^3$) and 59.7 $\mu g/m^3$ for O_3 (daily average was 54.4 $\mu g/m^3$). Almost all pollutant concentrations reached approximately twice the average in this period. Only O_3 concentrations remained low (Fig. 9). The dust transported from Sahara Desert was the main reason why particulate matter concentrations were increased.

Evaluation of meteorological parameters

The temperatures measured during the episode were above the average highest temperature of November (13.0 ℃) in Istanbul. This situation showed the weather conditions above the seasonal norms, which were caused by the southeast winds causing dust transport from the Sahara Desert and the high pressure was effective in Istanbul during the episode. During the period of time when the pollution was observed, wind speed values at surface level remained in the range of approximately 0.5–2.2 m/s. The prevailing wind direction throughout the episode was determined as northeast and southeast at the surface level. The pressure at surface level throughout the episode was calculated to be approximately 1006 hPa. This value, which was higher than the pressure values before and after the episode, indicated the presence of

high pressure. Looking at upper atmospheric levels (500 hPa level), the dominance of atmospheric blocking was observed over the region. This system, which prevailed between November 7 and November 26, left the region under the influence of high pressure. Thus, the rate of pollutant dispersion was also decreased.

WRF model results

In this section, first, WRF model's wind speed value outputs were analysed (Fig. 12). In the daily distribution of hourly data over five different vertical levels, it was observed that the wind speed values increased since the levels were above 30 m. Average wind speed values observed at each level throughout the episode were 2.53 m/s for 30 m, 3.09 m/s for 60 m, 3.68 m/s for 90 m, 4.10 m/s for 120 m and 5.32 m/s for 240 m. Maximum wind speed values emerged at all levels between 1350 and 2010 UTC (Universal Time Coordinated) on November 16, 2019. Maximum wind speed values observed at each level were 6.66 m/s for 30 m, 7.89 m/s for 60 m, 9.18 m/s for 90 m, 9.95 m/s for 120 m and 12.14 m/s for 240 m (Fig. 10).

WRF model wind direction data analyses were performed for five different vertical atmospheric levels (Fig. 10a–e). At 30 m level, the primary dominant wind direction was Northeast and the secondary dominant wind direction was Southwest. Although basically similar characteristics were observed toward the upper levels, distortions appeared in the dominant wind directions.
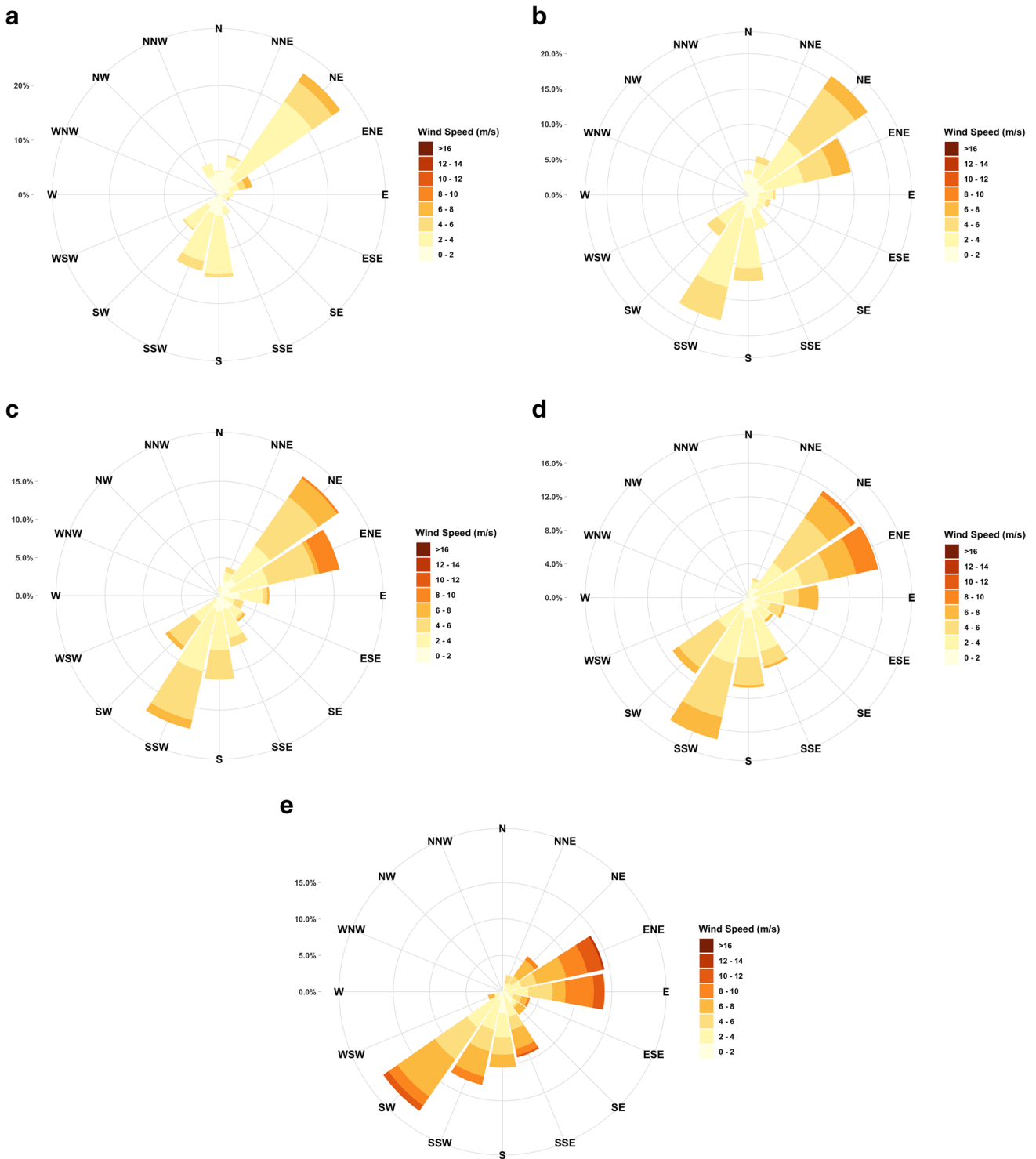
Fig. 10 Wind direction information at **a** 30 m, **b** 60 m, **c** 90 m, **d** 120 m, **e** 240 m vertical levels from WRF model outputs

SODAR results

The diurnal variations of the wind speed values obtained from the SODAR throughout the episode are shown in Fig. 12. In the daily distribution of hourly data over the period at five different vertical levels, it was observed that the wind speed values increased as the levels above the 30 m level increase, just like in the WRF model results. Average wind speed values observed at each level throughout the period were 3.67 m/s at 30 m, 4.36 m/s at 60 m,
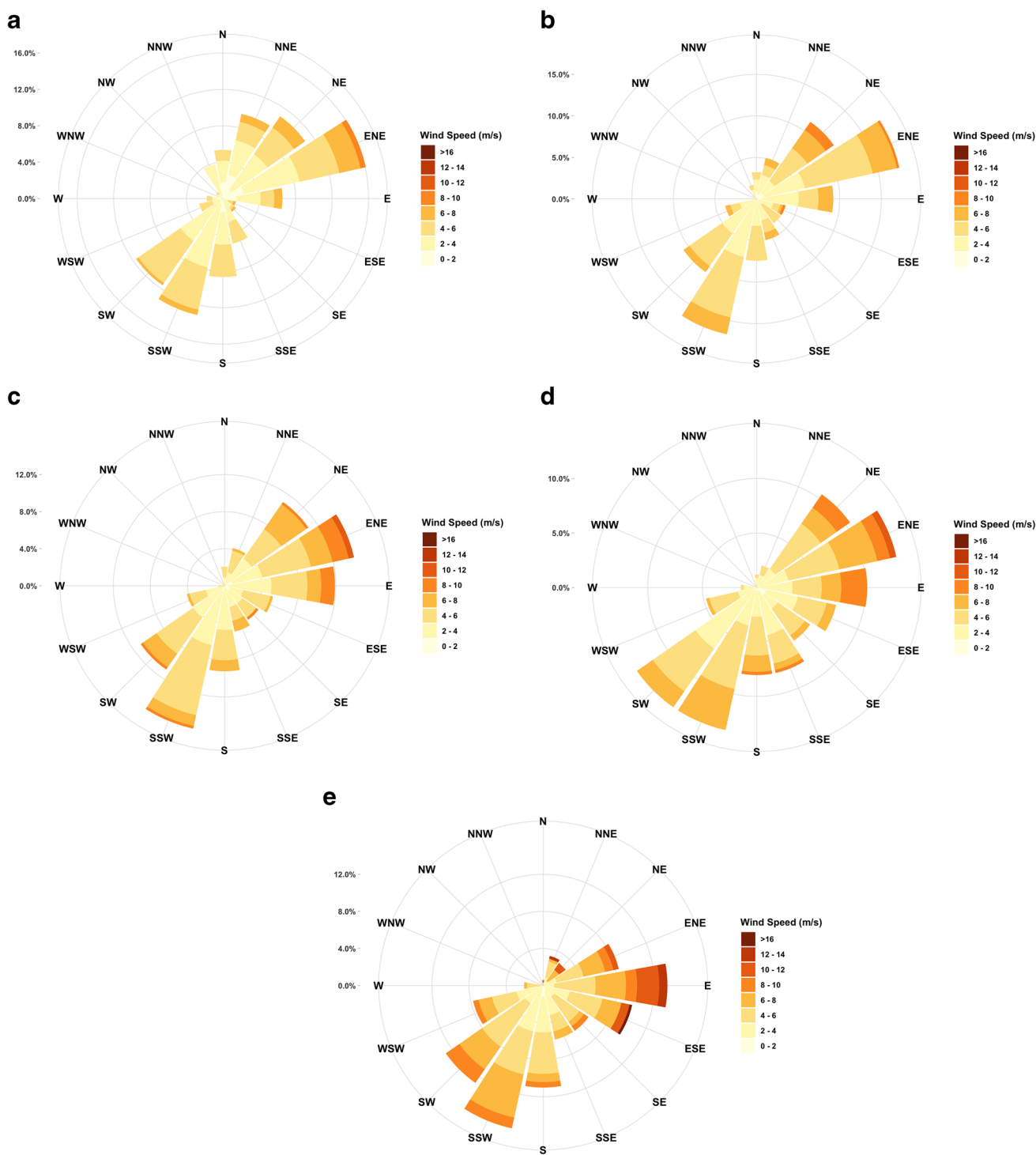
a

b

c

d

e

Fig. 11 The wind direction information at **a** 30 m, **b** 60 m, **c** 90 m, **d** 120 m, **e** 240 m vertical levels from SODAR

4.66 m/s at 90 m, 4.81 m/s at 120 m and 5.59 m/s at 240 m. Maximum wind speed values emerged at all levels between 1900 and 2000 UTC on November 16, 2019. Maximum wind speed values observed at each level were 8.38 m/s at 30 m, 9.69 m/s at 60 m, 10.20 m/s at 90 m, 10.85 m/s at 120 m and 14.10 m/s at 240 m.
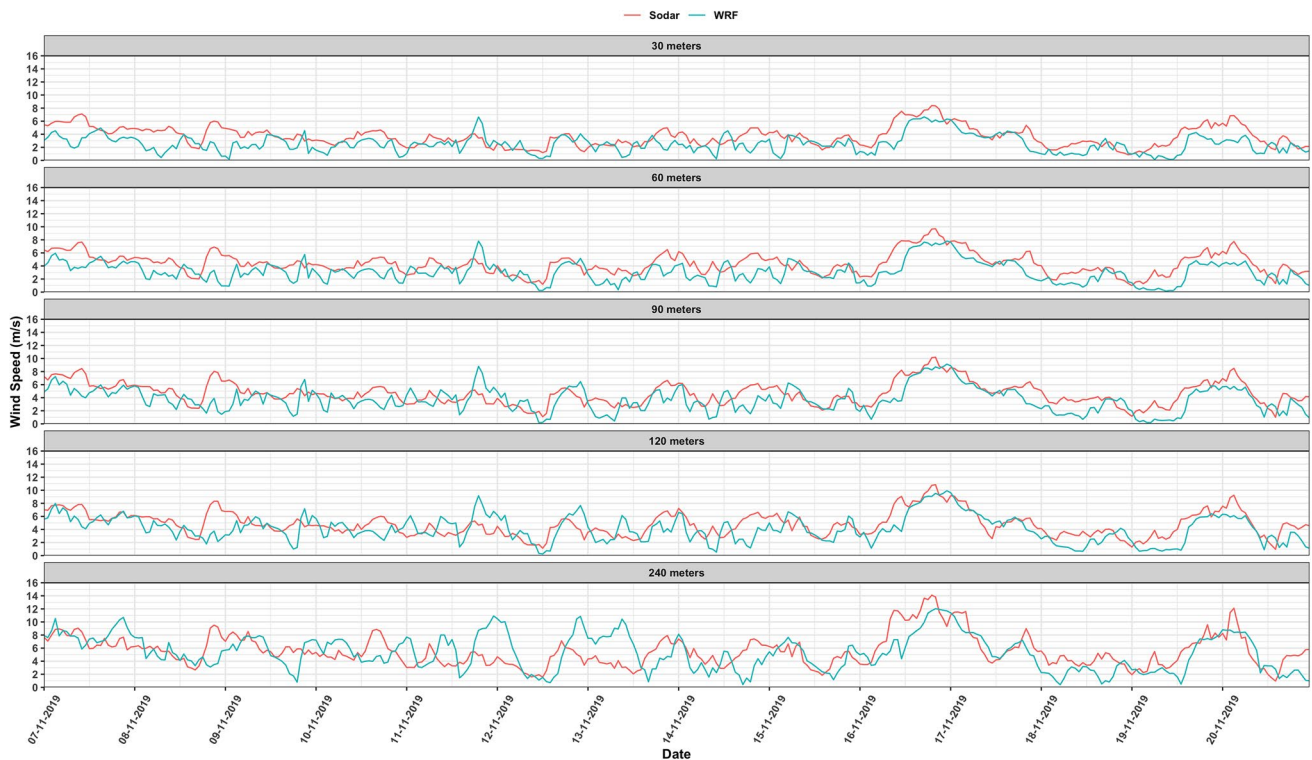
Fig. 12 The comparison of wind speed values obtained from WRF model and SODAR

Table 5 Statistical information about comparing two data types

Altitude	Correlation (Pearson)	RMSE	MAE
30 m	0.58	1.74	1.37
60 m	0.69	1.78	1.43
90 m	0.68	1.73	1.35
120 m	0.69	1.69	1.34
240 m	0.62	2.34	1.78

Analyses of wind direction values from SODAR were performed for five different vertical levels (Fig. 11). At 30 m level, the primary dominant wind direction was Northeast and the secondary dominant wind direction was South-Southwest. Although basically similar characteristics were observed toward the upper levels, distortions appeared in the dominant wind directions.

Comparison of the WRF model and SODAR results

The comparison of wind speed values obtained from WRF model and SODAR during the episodic days is given in Fig. 12. The error metrics for the relevant comparison are also included in Table 5. While very similar values were observed at the levels close to the surface, as it can be seen from the error metrics, there were differentiations towards the upper levels.

The comparison of the wind direction information obtained from WRF model and SODAR during the episodic days is given in Fig. 13. It was possible to see an almost overlapping resemblance at 30 m level. Although the prevailing wind direction was the same, minor changes were observed in the secondary prevailing directions. The consistency between the two data increased as the levels rose. Especially at 240 m level, primary and secondary prevailing wind directions coincided almost exactly with other prevailing wind directions. Inconsistencies between observation and model results especially for wind direction at close to surface levels were expected due to the friction effect at these layers and spatial resolution of the model.

As a result, it was found out that WRF model outputs can generally represent the wind speed and direction in accordance with measurements by SODAR. In addition to this, the high correlation between WRF outputs and SODAR measurements indicates linear relationship so that the representativeness of WRF outputs for observations can be increased by using a simple linear model. Besides, it should be highlighted that nonlinear machine learning methods such as tree-based models can also be used if there are sufficient data for training purposes.
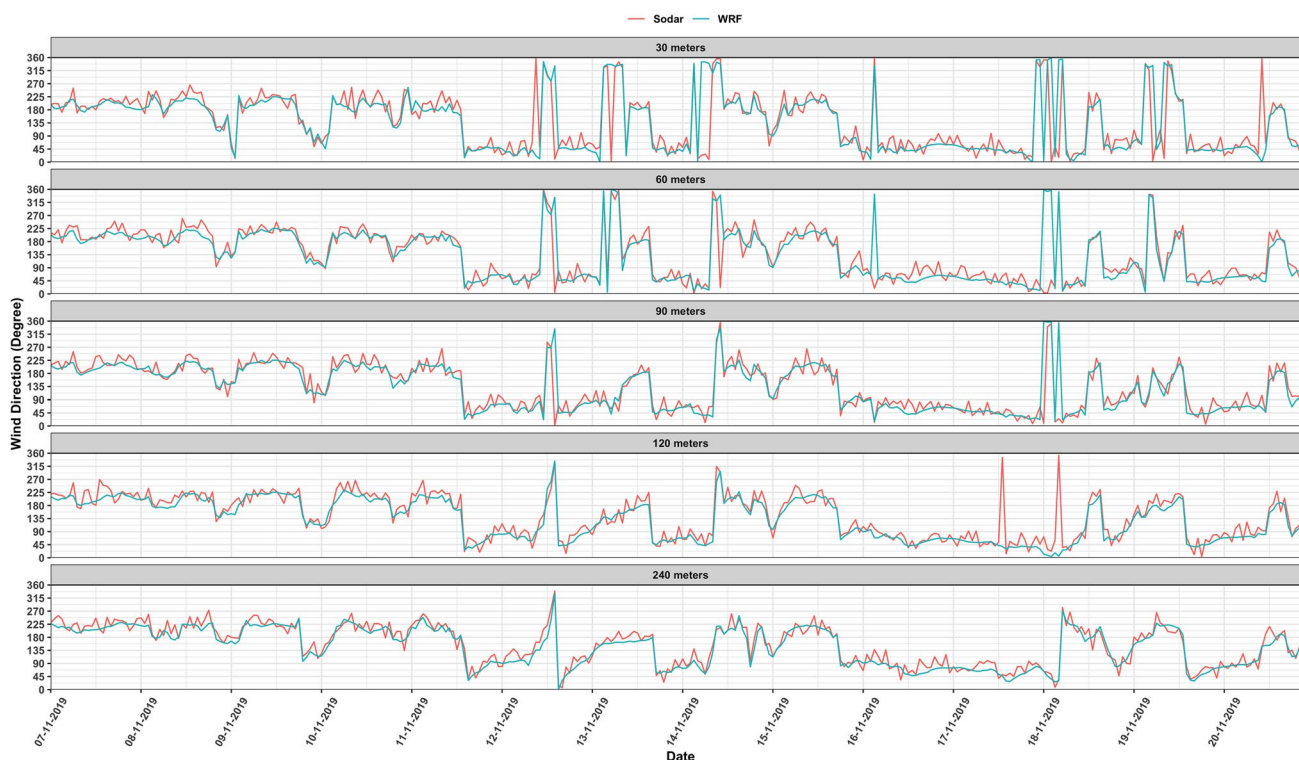
Fig. 13 The comparison of wind direction data obtained from WRF model and SODAR. The oscillations of hourly data at 30 m, 60 m, 90 m, 120 m and 240 m vertical levels on a daily basis

On the other hand, while low PM10 concentrations were observed on November 12 and 17, 2019, high concentrations were observed on November 14 and 19, 2019 based on the selected episode days shown in Fig. 9. High pollutant concentrations have been observed on November 14 and 19, 2019 during which vertical wind shear is quite low and atmosphere can be classified as stable. Daily wind speeds at 30, 60, 90, 120 and 240 m heights are 2.27, 2.67, 3.11, 3.21, 3.46 m/s and 1.76, 2.01, 2.37, 2.78, 3.9 m/s on November 14 and 19. Furthermore, Peña et al. (2014) have showed that the wind veers under barotropic conditions especially in neutral and stable atmospheric conditions within the atmospheric boundary layer. The wind veering has been observed on November 14 and 19 according to the wind direction measurements that can be seen in Fig. 13. Daily wind speeds at 30, 60, 90, 120 and 240 m heights are 2.25, 2.8, 3.41, 3.9, 5.17 m/s and 3.74, 4.46, 5.17, 5.81, 6.89 m/s on 12 and 17 November. High wind shear was also observed on these days and it indicates the presence of mechanical turbulence within the atmospheric boundary layer. Mechanical turbulence leads to better mixing of the atmosphere and this can reduce the concentration of the air pollutants at the surface level with the mixing effect.

Ceilometer results

Throughout the episode days, cloud coverage amount and cloud base height data were obtained from the ceilometer with 10-min intervals. Data obtained from the device were analysed for both data types at four different vertical levels. In terms of cloud coverage, the average coverage was calculated as 0.92/8; 0.17/8 at level 1 and at level 2; 0.005/8. No cloud information was detected by the device at level 4. The dates when cloud coverage amounts were observed in the range of 7/8–8/8 at high coverage rates were November 11, 2019, November 14, 2019 and November 20, 2019. In the analysis for cloud base heights, the average cloud base height at level 1 was 2221 m, at level 2 it was 1669 m and at level 3 it was 1626 m. Since no cloud information at level 4 was detected by the device, there was no cloud base height data at this level (Fig. 14). Although high pressure effect was observed due to atmospheric blocking during the episode, short-term heavy rainfalls also occurred in most of the days (this information was obtained from the aviation reports published by Istanbul Atatürk International Airport and Istanbul Sabiha Gökçen International Airport). On November 11, 14 and 20, 2019, wind speeds varied in the range of 1–8 m/s at surface level, and 4–14 m/s at 240 m level. On these days, both the WRF Model and the SODAR data gave similar wind speed results. The Ceilometer results

Fig. 14 The cloud base heights during the episode
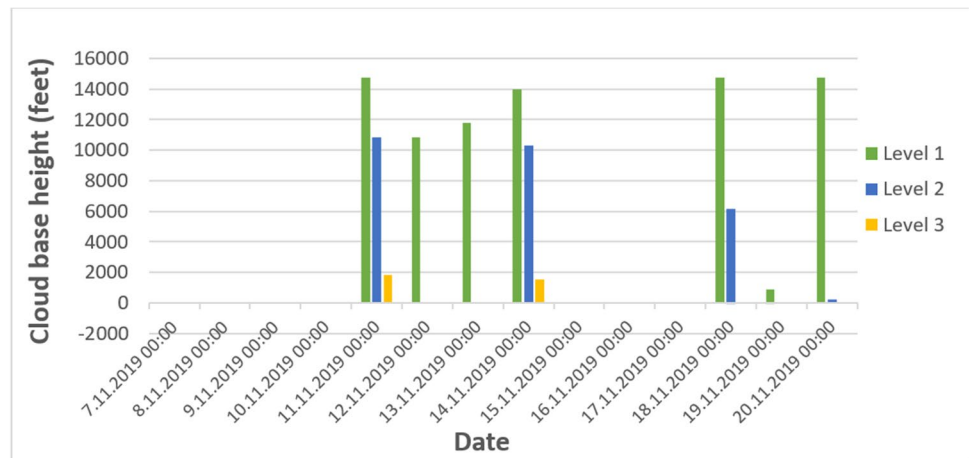
showed that the cloud base height could be determined at three different vertical levels on similar dates, and the first level was around 15,000 ft. looking at the reports published by airports, on November 11, 2019, occasional heavy rainfall occurred in the city. On November 14, 2019, rain showers were observed occasionally in the early hours of the day and haze occurred in the evening hours. Similar atmospheric conditions happened on November 20, 2019. The data obtained from both the WRF Model and SODAR on November 11, 14 and 20, 2019, show that the near-surface and upper level wind speeds were higher than the other days. The Ceilometer provided accurate calculations in terms of cloud coverage and cloud base height information on these aforementioned days. Both remote sensing devices and the WRF Model demonstrated the consistency of their output.

On the other hand, on 7.11.2019 while east and central regions of Turkey were under the effect of high pressure center at 1020 hPa, west regions of Turkey are exposed to frontal systems sectors (an expression that is used to address the field between cold front and warm front) that range from the Balkans, east of the Sicily island to north Africa. Generally, pressure value is at 1014 hPa. Correspondingly, while winds in Istanbul blow from south at generally 5–8 knots, the weather is completely clear. In accordance with the pattern in this synoptic scale, on the specified day the Ceilometer did not measure any value. Until November 11, 2019 00:00 UTC aforementioned synoptic pattern has continued to affect the region. Therefore, up until November 11, 2019, Ceilometer did not measure any cloud height. On November 11, effects of the high pressure were increased and it rose up to 1020 hPa. Again on this date, cloudiness of the frontal system which reaches from Bulgaria to Peloponnese effected Istanbul and it was mostly under the influence of mid and low level clouds.

Similar synoptic patterns have continued to be effective and Istanbul remained in the sector (for the duration of 12th and 13th of November). As a result of this, at times

mid-level clouds have emerged. On 14th of November at 06:00 UTC, there is a low pressure center with 1010 hPa located on North Aegean (not shown on the map). On this day, it rained heavily in Istanbul and mid and low level clouds were formed. In Istanbul, on 15th of November pressure value was at 1022 hPa, on 16th it was at 1023 hPa and on 17th it was at 1021 hPa which means Istanbul got into high pressure system effect. Since there was no cloud formation on these aforementioned dates, Ceilometer did not make measurements. On 18th, 19th and 20th again, Istanbul was still under the influence of high pressure. On the 19th of November, pressure value was at 1025 hPa. On this 3 days, generally mid-level clouds were formed and from time to time low level clouds was also observed.

Consequently, in the 13-day period during which Ceilometer measurements were made, mostly high pressure conditions were present in Istanbul and it rained only once, on the days other than that one the weather was clear. On cloudy days, there were mostly mid-level clouds and occasionally low level clouds were observed.

During a 6-year period of time between March 1, 2013 and March 1, 2019, Özdemir et al. (2020) did not see a correlative relationship in their studies based on Istanbul between hourly pressure changes and hourly average PM10 values on the days in which highest and lowest pressure values were measured. This incident points out to the fact that changes in PM10 values are not directly related to pressure; it shows that there are incidents which can be effected by other meteorological parameters.

On the days during which Ceilometer measurements were made, there were no significant changes in PM10 values and it cannot be said that these changes increase or decrease depending solely on pressure or a slight cloudiness formation.

Fig. 15 Mean sea level pressure (hPa) and wind flags (knots) map of Europe at 09:00 UTC on November 4, 2019 (NOAA, 2021)
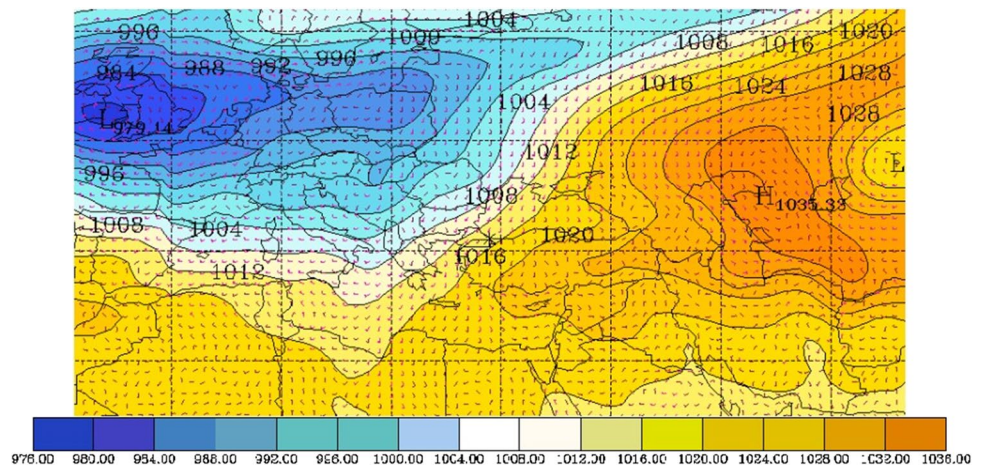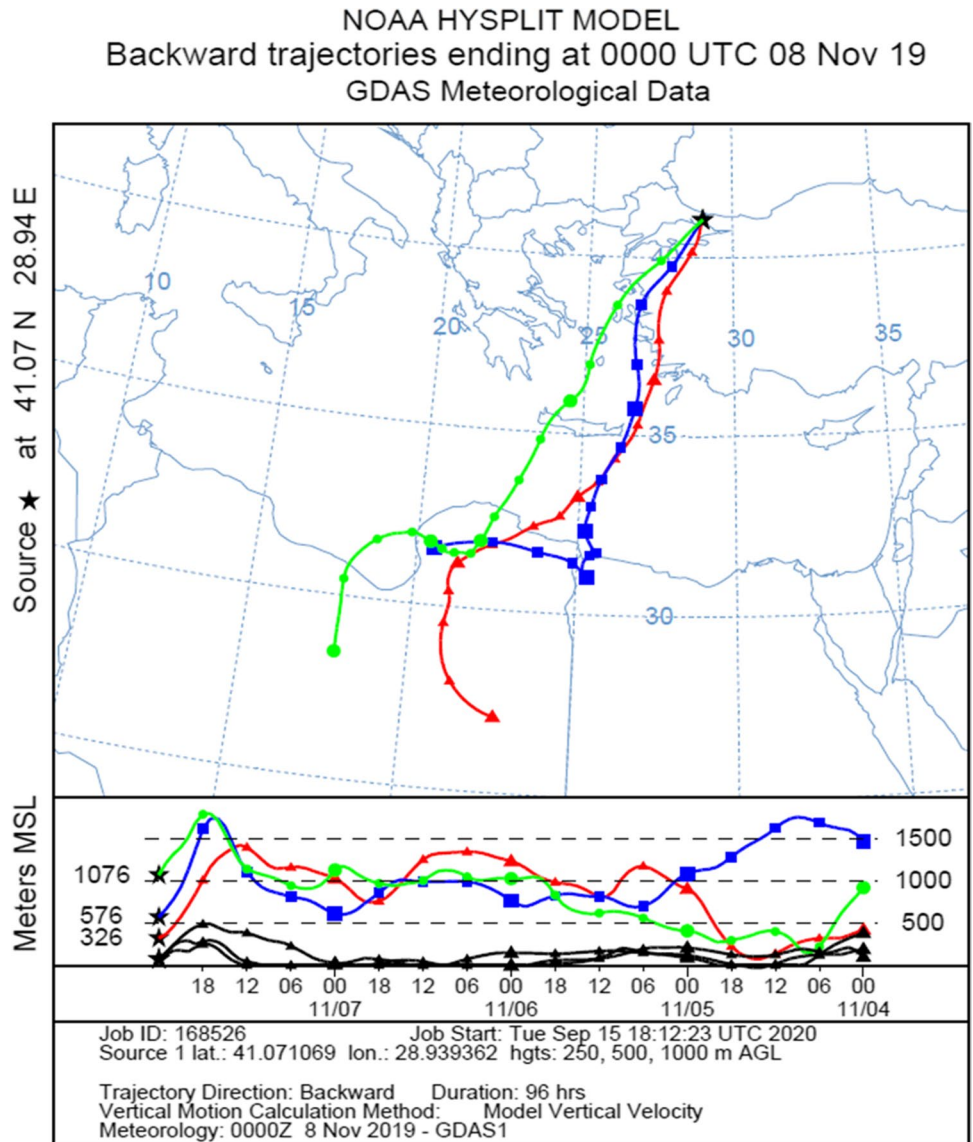

Fig. 16 Dust transport on November 8, 2019

HYSPLIT system results

On November 4, 2019, a cyclone centred on Western England with a 979-hPa low-pressure centre caused a southerly wind event on the eastern Mediterranean (Fig. 15). Desert sands lifted by strong winds hovered off the coasts of North Africa and spanned the Mediterranean, and reached Istanbul. The dust storm hit the Marmara, Aegean, Mediterranean regions of Turkey. According to the historical trajectory analysis of the HYSPLIT system, which was produced for November 8, 2019 and operated for 96 h backwards from 0000 UTC, the increase of particulate matter (PM_{10} and $PM_{2.5}$) concentrations in Istanbul on the specified date was caused by dusts originating from the Sahara Desert (Fig. 16). Figure 16 shows that 0000 UTC HYSPLIT 4-day back trajectories started over Libya at 1000, 500 and 250-m heights on November 4, 2019 and reached Istanbul on November 8, 2019.

Results and discussions

In this study, negative correlations were found between wind speed/temperature and PM concentrations, and positive correlations were found between surface pressure/relative humidity and PM concentrations. Many studies have been discussed in the "Introduction" section regarding that low wind speed values and stable atmospheric conditions will adversely affect dispersion. Therefore, in terms of atmospheric conditions in Istanbul, wind direction and speed patterns play a major role in high concentrations of air pollutants.

During the examinations throughout the episode, low wind speeds, high pressure values and minor wind direction changes were observed in Kagithane AQMS. Similarly, in the measurements made by the SODAR both at the surface and above surface levels, the wind speed values and changes in direction were low. According to the data obtained from the Ceilometer, the high cloud base height and the very low amount of cloud coverage show that Istanbul was dominated by high pressure system or ridge point. In the examinations made with the upper atmospheric level charts, the presence of atmospheric blocking at the 500 hPa level was detected. Atmospheric blocking plays an important role for modifying the weather of a region located under the blocked area. Atmospheric blocking affects the precipitation (Efe et al. 2019) and temperature (Efe et al. 2020a, 2020b) values over Turkey. Turkey was also under the influence of atmospheric blocking during the period. There was a long-lasting atmospheric blocking event that covers the study period according to the blocking archive used in Lupo et al. (2019). It started on November 7, 2019 and ended on November 26, 2019. The duration of this blocking was two times greater than the average span of blocking events in fall. Mean size of blocking was 3295 km, which is greater than the average size of blocking events that influence the regions around Turkey in fall. The type of blocking was omega since the shape of the waves is similar to the Greek letter omega. The mean blocking intensity was 3.78 which is classified as strong blocking according to Wiedenmann et al. (2002). Turkey was under the influence of high pressure located over the North-east of Turkey during the blocking that causes a downward motion for air pollutants. In the HYSPLIT system review, dust transport from the Sahara Desert was detected at the episode. Both the Sahara dust transport that happened just before the atmospheric blocking dominance over the region, and long-term dominance of blocking caused an increase in the concentration values, especially by preventing the distribution and transport of PM.

In air pollution studies using the SODAR, wind shears and turbulence structures (e.g. clear air turbulence) that emerge due to the change of humidity and based on temperature of the atmosphere have been examined (Marc et al. 2015). Mölders et al. (2011) made comparisons using the SODAR, radiosonde data and WRF-Chem model to reveal the characteristics of ABL. As a result, it has been revealed that the WRF-Chem model predicts wind speeds roughly in accordance with the ABL than the SODAR data. Especially in the presence of low-level jets, these differences were increased. In comparison of the SODAR and radiosonde wind speed data at 10 m, high compatibility was observed. In the WRF-Chem model, the presence of synoptic and local scale forcings led to an increase in inconsistency in terms of wind speed and persistence. Emeis et al. (2004) used the SODAR and the Ceilometer to examine the ABL changes. It was revealed that the SODAR was effective in the analysis of the convective boundary layer (CBL) and in revealing its top in the first half of the day, and in the second half when the convectivity increased, effective results could not be obtained because the top of the CBL was out of the range. For this reason, the Ceilometer was used to assess the MLH and the CBL top for the second half of the day. It has been demonstrated that it can be determined with high accuracy by both the SODAR and the Ceilometer at night, especially when surface inversion occurs at lower atmospheric levels (100 m). In addition, the Ceilometer did not produce useful data in high cloud coverage and when there is rain or snow. Keder et al. (2004) used SODAR's 3 years' measurement data in their study and decided that the device was functional in revealing the wind characteristics of the atmosphere along the vertical column near the ground and in evaluating the pollutant concentrations associated with it. Also, the Ceilometer is suitable for studying the vertical structure of the atmosphere below the lowest cloud layer in the absence of rain and heavy fog, and in the absence of strong turbulent mixing and high wind speeds. The optimum conditions for

both devices to operate in combination are low-to-moderate wind speeds (up to 10–15 m/s maximum), shallow layers that appear at night (surface inversion) and the convective boundary layer (up to 500 m from the surface) in the early hours of the day (Emeis et al. 2009). In this study, the average wind speed at surface level was in the range of 0–9 m/s. For this reason, complications were not encountered in the data obtained from both the SODAR and the Ceilometer related with this phenomenon. Also, on some days with high wind speeds, compatibility between the SODAR and the WRF model outputs remained intact. Rainfall and unstable atmospheric conditions in spring, autumn and early summer caused incompatibility between the SODAR data and the WRF model outputs, especially in determining wind speed and direction. On days with no precipitation, low-to-moderate wind speeds, the data obtained from the SODAR up to 240 m level showed one-to-one correspondence with the WRF model results at near-surface level. Therefore, for these levels where surface roughness, local and topographic effects cause serious changes; the WRF model gave high consistency results for the city. Similarly, the cloud height data obtained from the Ceilometer in the afternoon hours when convectivity was increased were compatible with the WRF model in stable atmospheric conditions (except for dense fog), while over/under wind speed estimation in unstable atmospheric conditions (precipitation and high wind speeds/shears).

Conclusions

After choosing the episode days by considering the Sahara Desert dust and the air pollutant concentrations taken from Şirinevler AQMS, PM10 has been chosen as the pollutant of the study. SODAR and LIDAR remote sensing devices were used in order to understand the atmospheric conditions and to define atmospheric stability during the selected episode days and with the aim of making synoptic analysis. By using the wind speed and direction data taken from SODAR, the stability of the atmosphere was determined daily. Hence, it has been observed that the PM10 concentration is high when the atmosphere is stable. On the other hand, no direct relationship was found between the cloud base heights measured with the ceilometer and PM10 concentrations.

The prominent results of the study are as follow: dust transport from the Sahara Desert was the main reason for the high concentrations of air pollutants that transpired during the episode. The dominance of the atmospheric blocking observed in the mid-troposphere over the region during the episode prevented the distribution of pollutants. In unstable atmospheric conditions emerged on only a few days during the episode, a decrease in pollutant concentrations was observed due to the moderate wind speeds and rain showers.

As a result of the investigations, it was determined that local and synoptic scale analyses are important in determining the source of pollution and its trajectory/distribution. It has been decided that SODAR and Ceilometer remote sensing devices will be used to understand the general condition and to determine the stability of the atmosphere. A few days of occasional rain showers could be detected with the help of the SODAR and the Ceilometer. This shows that the devices are of great importance in terms of revealing atmospheric conditions in air pollution research. Similarly, the use of the HYSPLIT system in detecting the source and trajectory of the pollutant, the configuration of the WRF Model over the area and the SODAR providing consistent results at near-ground levels are important in terms of determining the scale/duration/trajectory of air pollution. It will form an important basis for future studies and the creation of predictive models for pollution concentrations.

Author contribution ● Veli Yavuz has no relevant financial or non-financial interest to disclose.
    ● Cem Özen has no relevant financial or non-financial interest to disclose.
    ● Özkan Çapraz has no relevant financial or non-financial interest to disclose.
    ● Emrah Tuncay Özdemir has no relevant financial or non-financial interest to disclose.
    ● Ali Deniz has no relevant financial or non-financial interest to disclose.
    ● İbrahim Akbayır has no relevant financial or non-financial interest to disclose.
    ● Hande Temur has no relevant financial or non-financial interest to disclose.

Declarations

References

Angevine WM, Senff CJ (2015) Observational technique: remote. Revision of the previous edition article by Angevine, Senff Westwater. 1:271–279, © 2003, Elseiver Ltd.

Avdakovic S, Dedovic MM, Dautbasic N, Dizdarevic J (2016) The influence of wind speed, humidity, temperature and air pressure on pollutants concentrations of PM10—Sarejevo case study using wavelet coherence approach. XI International Symposium on Telecommunications (BIHTEL). Sarejovo, Bosnia and Herzegovina. 24–26 October, 2016

Beyrich F, Görsdorf U (1995) Composing the diurnal cycle of mixing height from simultaneous SODAR and wind profiler measurements. Bound Layer Meteorol 76:387–394. https://doi.org/10.1007/BF00709240

Biral (2020) CBME80B cloud ceilometer datasheet. https://www.biral.com/wp-content/uploads/2015/07/CBME80B-CLOUD-CEILOMETER-DS-DOC101422.01A.pdf Accessed 10 Sep 2020

Coulter RL (1979) A comparision of three methods for measuring mixing layer height. J Appl Meteorol 18:1495–1499. https://doi.org/10.1175/1520-0450(1979)0182.0.co;2

Çapraz Ö, Efe B, Deniz A (2016) Study on the association between air pollution and mortality in İstanbul, 2007–2012. Atmos Pol Res 7(1):147–154. https://doi.org/10.1016/j.apr.2015.08.006

Çapraz Ö, Deniz A, Doğan N (2017) Effects of air pollution on respiratory hospital admissions in İstanbul, Turkey, 2013 to 2015. Chemosphere 181:544–550. https://doi.org/10.1016/j.chemosphere.2017.04.105

Çapraz Ö, Deniz A (2020) Particulate matter (PM_{10} and $PM_{2.5}$) concentrations during a Saharan dust episode in Istanbul. Air Qual Atmos Health. https://doi.org/10.1007/s11869-020-00917-4

DeSouza P (2020) Air pollution in Kenya: a review. Air Qual Atmos Health 13:1487–1495. https://doi.org/10.1007/s11869-020-00902-x

Devera PCS, Ernest Ray P, Murthy BS, Pandithurai G, Sharma S, Vernekar KG (1995) Intercomparison of nocturnal lower atmospheric structure observed with LIDAR and SODAR techniques at Pune. Indian J Appl Meteorology 34:1375–1383. https://doi.org/10.1175/1520-0450(1995)034%3c1375:IONLAS%3e2.0.CO;2

Efe B, Lupo AR, Deniz A (2019) The relationship between atmospheric blocking and precipitation changes in Turkey between 1877 and 2016. Theor Appl Climatol 138(3–4):1573–1590. https://doi.org/10.1007/s00704-019-02902-z

Efe B, Sezen İ, Lupo AR, Deniz A (2020a) The relationship between atmospheric blocking and temperature anomalies in Turkey between 1977–2016. Int J Climatol 40(2):1022–1037. https://doi.org/10.1002/joc.6253

Efe B, Lupo AR, Deniz A (2020b) Extreme temperatures linked to the atmospheric blocking events in Turkey between 1977 and 2016. Nat Hazards 104(2):1879–1898. https://doi.org/10.1007/s11069-020-04252-ws

Emeis S, Münkel C, Vogt S, Müller WJ, Schafer K (2004) Atmospheric boundary layer structure from simultaneous SODAR, RASS and ceilometer measurements. Atmos Environ 38:273–286. https://doi.org/10.1016/j.atmosenv.2003.09.054

Emeis S, Schaefer K, Münkel C (2009) Observation of the structure of the urban boundary layer with different ceilometers and validation by RASS data. Meteorol Z 18(2):149–154. https://doi.org/10.1127/0941-2948/2009/0365

Freedman JM, Fitzjarrald DR, Moore KE, Skai RK (2001) Boundary layer clouds and vegetation atmosphere feedbacs. J Clim 12(2):180–197. https://doi.org/10.1175/1520-0442(2001)013%3c0180:BLCAVA%3e2.0.CO;2

Gera BS, Singh G, Ojha VK, Saxena N, Gupta PK, Dutta HN (2000) Studies of boundary layer parameters and air pollution concentration at different traffic junctions. Proceedings of 10th Symp. ISARS, (pp.256–259). New Zealand/Auckland, 26 Nov – 1 Dec

Gurjar BR, Lelieveld J (2005) New directions: megacities andglobal change. Atmos Environ 39:391–393. https://doi.org/10.1016/j.atmosenv.2004.11.002

Gurjar BR, Butler TM, Lawrence MG, Lelieveld J (2008) Evaluation of emissions and air quality in megacities. Atmos Environ 42(7):1593–1606. https://doi.org/10.1016/j.atmosenv.2007.10.048

Guttikunda SK, Carmichael GR, Calori G, Eck C, Woo JH (2003) The contribution of megacities to regionalsulfur pollution in Asia. Atmos Environ 37:11–22. https://doi.org/10.1016/S1352-2310(02)00821-X

Iacono MJ, Delamere JS, Mlawer EJ, Shephard MW, Clough SA, Collins WD (2008) Radiative forcing by long-lived greenhouse gases: Calculations with the AER radiative transfer models. J Geophys Res 113:D13103. https://doi.org/10.1029/2008JD009944

IMM (İstanbul Metropolitan Municipality) Environmental Protection and Control Department (2020) Measuring devices. https://havakalitesi.ibb.gov.tr/Icerik/hakkimizda/olcum-cihazlari Accessed 30 September 2020

İncecik S, İm U (2012) Air pollution in mega cities: a case study of Istanbul. Air pollution - monitoring, modelling and health. Intech Open Access Publisher, 77–116

Janjic ZI (1994) The step-mountain eta coordinate model: further developments of the convection, viscous sublayer, and turbulence closure schemes. Mon Wea Rev 122(5):927–945. https://doi.org/10.1175/1520-0493(1994)122%3c0927:TSMECM%3e2.0.CO;2

Keder J, Berger P, Cerny A, Engst P, Folttiny F, Strizik M (2002) Operational measurement of air pollution concentrations in the Czech 90 Republic by combined LIDAR/SODAR techniques. Proceedings of 11th Symp. ISARS, (pp. 417–422). Italy: CNR/Rome, June 24–28

Keder J, Strizik M, Berger P, Cerny A, Engst P, Nemcova I (2004) Remote sensing detection of atmospheric pollutants by differential absorption LIDAR 510M/SODAR PA2 mobile system. Meteorol Atmos Phys 85:155–164

Lawrence MG, Butler TM, Steinkamp J, Gurjar BR, Lelieveld J (2007) Regional pollution potentials of megacities and other major population centers. Atmos Chem Phys 7:3969–3987. https://doi.org/10.5194/acp-7-3969-2007

Li Y, Chen Q, Zhao H, Wang L, Tao R (2015) Variations in PM10, PM2.5 and PM1.0 in an urban area of the sichuan basin and their relation to meteorological factors. Atmosphere 6(1):150–163. https://doi.org/10.3390/atmos6010150

Liu Z, Yu L (2020) Stay or Leave? The role of air pollution in urban migration choices. Ecological Economics 177https://doi.org/10.1016/j.ecolecon.2020.106780

Lupo AR, Jensen AD, Mokhov II, Timazhev AV, Eichler T, Efe B (2019) Changes in global blocking character in recent decades. Atmosphere 10(92). https://doi.org/10.3390/atmos10020092

Maciejewska K (2020) Short-term impact of PM2.5, PM10, and PMc on mortality and morbidity in the agglomeration of Warsaw. Poland Air Qual Atmos Health 13:659–672. https://doi.org/10.1007/s11869-020-00831-9

Marc M, Tobiszewski M, Zabiegala B, de la Guardia M, Namiesnik J (2015) Current air quality analytics and monitoring: a review. Anal Chim Acta 853:116–126. https://doi.org/10.1016/j.aca.2014.10.018

Marsik FJ, Fischer KW, McDonald TD, Samson PJ (1995) Comparison of methods for estimating mixing layer height used during the 1992 Atlanta field initiative. J Appl Meteorol 34:1802–1814. https://doi.org/10.1175/1520-0450(1995)034%3c1802:COMFEM%3e2.0.CO;2

MEU (Ministry of Environment and Urbanization) (2008) Air quality assessment and management regulation. https://www.resmigazete.gov.tr/eskiler/2008/06/20080606-6.htm Accessed 16 September 2020

Monin AS, Obukhov M (1954) Basic laws of turbulent-mixing in the surface layer of the atmosphere. Contrib Geophys Inst Acad Sci USSR 151:163–187 ((**in Russian**))

NOAA (2020) HYSPLIT atmospheric transport and dispersion modeling system. https://www.ready.noaa.gov/HYSPLIT.php. Accessed 22 September 2020

Özdemir ET, Deniz A, Yavuz V, Çiftçi ND, Akbayır İ (2018) Investigation of the air quality relationship in İstanbul. Fresen Environ Bull 27(1):30–36

Özdemir ET, Çapraz Ö, Deniz A (2020) Investigation of the relationship between extreme pressure values and particulate matter (PM10) values for megacity Istanbul. J Anatolian Environ Animal Sci 5(4):484–490

Öztürk M (2017) Temperature inversion increasing air pollution. http://www.cevresehirkutuphanesi.com/assets/files/slider_pdf/ro17bNm6ttR8.pdf. Accessed 18 Sep 2020 **(in Turkish)**

Peña A, Gryning S E, Floors R (2014) The turning of the wind in the atmospheric boundary layer. Journal of Physics: Conference Series (Vol. 524, No. 1, p. 012118). IOP Publishing. https://doi.org/10.1088/1742-6596/524/1/012118

Peng J, Grimmond CSB, Fu X, Chang Y, Zhang G, Guo J, Tang C, Gao J, Xu X, Tan J (2017) Ceilometer-based analysis of Shangai's boundary layer Height (under rain and fog free conditions). J Atmos Ocean Tech 34(4):749–764. https://doi.org/10.1175/JTECH-D-16-0132.1

Remtech (2020). Remtech PA-O SODAR acoustic wind profiler. https://www.remtechinc.com/sites/default/files/inline-files/PA-0.pdf Accessed 24 Sep 2020

Rife DL, Davis CA (2005) Verification of temporal variations in mesoscale numerical wind forecasts. Mon Wea Rev 133:3368–3381. https://doi.org/10.1175/MWR3052.1

Schafer K, Jardines EF, Emeis S, Grutter M, Kurtenbach R, Wiesen P, Münkel C (2009) Determination of mixing layer heights by ceilometer and influences upon air quality at Mexico City airport. The International Society for Optical Engineeringhttps://doi.org/10.1117/12.830425

Signal SP (1993) Monitoring air pollution related meteorology using SODAR. Appl Phys B 57:65–82. https://doi.org/10.1007/BF00324102

Spiridonov V, Ancev N, Jakimovski B, Velinov G (2020) Improvement of chemical initialization in the air quality forecast system in North Macedonia, based on WRF-Chem model. Air Qual Atmos Healthhttps://doi.org/10.1007/s11869-020-00933-4

Stieb DM, Doiron MS, Blagden P, Burnett RT (2005) Estimating the public health burden attributable to air pollution: an illustration using the development of an alternative air quality index. J of Toxicology and Env Health, Part A 68(13):1275–1288

Teixeira J, Hogan T (2002) Boundary layer clouds in a global atmospheric model: simple cloud cover parametrizations. J Climate 15(11):1261–1276. https://doi.org/10.1175/1520-0442(2002)015%3c1261:BLCIAG%3e2.0.CO;2

Tewari MF, Chen F, Wang W, Dudhia J, LeMone MA, Mitchell K, Ek M, Gayno G, Wegiel J, Cuenca RH (2004) Implementation and verification of the unified NOAH land surface model in the WRF model. 20th conference on weather analysis and forecasting/16th conference on numerical weather prediction, pp.11–15.

Thompson G, Field PR, Rasmussen RM, Hall WD (2008) Explicit forecasts of winter precipitation using an improved bulk microphysics scheme: Part II: Implementation of a new snow parameterization. Mon Wea Rev 136:5095–5115. https://doi.org/10.1175/2008MWR2387.1

UNCSD (2001) Protection of the atmosphere-report to the secretary general. E/CN.17/2001/2, Commission for Sustainable Development, New York, USA

Unal YS, Toros H, Deniz A, Incecik S (2011) Influence of meteorological factors and emission sources on spatial and temporal variations of PM10 concentrations in Istanbul metropolitan area. Atmos Environ 45(31):5504–5513. https://doi.org/10.1016/j.atmosenv.2011.06.039

Wiedenmann JM, Lupo AR, Mokhov II, Tikhonova EA (2002) The Climatology of Blocking Anticyclones for the Northern and Southern Hemispheres: Block Intensity as a Diagnostic. Journal of Climate 15(23):3459–3473. https://doi.org/10.1175/15200442(2002)015<3459:TCOBAF>2.0.CO;2

Zhang C, Wang Y, Hamilton K (2011) Improved representation of boundary layer clouds over the Southeast Pacific in ARW-WRF using a modified Tiedtke Cumulus Parameterization Scheme. Mon Wea Rev 139(11):3489–3513. https://doi.org/10.1175/MWR-D-10-05091.1